ARCHIVES
of
FOUNDRY ENGINEERING

ISSN (2299-2944)

10.24425/afe.2025.155362

Published quarterly as the organ of the Foundry Commission of the Polish Academy of Sciences

Microstructural Fracture Mechanism of Normalising Heat Treated Low-Alloy Cast Steels under Tensile Stress Conditions

B. Garbarz *, W. Spiewok
Łukasiewicz Research Network - Upper Silesian Institute of Technology, Gliwice, Poland
* Corresponding author: e-mail: bogdan.garbarz@git.lukasiewicz.gov.pl

Received 29.01.25; accepted in revised form 17.04.25; available online 25.07.2025

Abstract

The microstructural fracture mechanism of normalising heat treated low-alloy medium-carbon cast steels having a pearlitic-ferritic or multiphase pearlitic-ferritic-martensitic-bainitic microstructure has been investigated using metallography and mechanical testing methods. Four experimental cast steels in the form of plates having dimensions of 400 mm x 135 mm x 15 mm obtained under laboratory conditions were tested. The porosity of the castings was determined using the comparative hydrostatic weighing method (Archimedes' method). The mean porosity of the investigated cast plates was in the range of 0.52-1.18%. The plates were normalised using austenitising temperature just above Ac_3, annealing time 30 minutes and various rates of cooling, what resulted in multiphase microstructure. For characterisation of mechanical properties in as cast and heat treated conditions tensile tests and hardness measurements were carried out. As a result of optimisation of chemical composition and normalising parameters of the experimental cast steels yield strength reached 407-440 MPa, tensile strength attained 586-601 MPa and elongation amounted to 6-8%. The obtained mechanical properties are higher than properties of standard grades of structural cast steels in normalised condition. The microstructure was observed and described using light microscopy and scanning electron microscopy. The phenomenon of fracture in pearlitic-ferritic areas takes place through the coalescence of newly formed cracks and existing cavities, producing dimple-cleavage morphology of fracture surface. In martensitic and bainitic areas, the propagation of fracture results from the growth and coalescence of newly formed cracks.

Keywords: Cast steels, Multiphase microstructure, Crack nucleation, Fracture mechanism

1. Introduction

The primary difference in the macro and microstructure of steel castings and steel products manufactured using the plastic working technology is that castings contain material discontinuities in the form of shrinkage cavities as well as the micro and macrosegregation of chemical elements characterised by greater intensity than those in plastically deformed products. The segregations of chemical elements formed during solidification are responsible for the microstructural inhomogeneity and the non-uniform distribution of non-metallic inclusions in castings [1]. Castings may also contain gas-induced porosity, thermal cracks and exogenous inclusions (inclusions of moulding sand and slag). In terms of their size, the above-named discontinuities and inclusions can be divided into microscale, mesoscale (i.e. intermediate size) and macroscale ones. In addition, discontinuities and inclusions can also be divided in relation to their morphological form (shape). The size and shape of discontinuities depend on types of cast alloys, solidification mechanisms and conditions as well as the size and shape of castings [2]. Research works were carried out to modify the macrostructure and microstructure of castings by affecting the rate of solidification and cooling following solidification (e.g. [3]).

However, in many cases, there are no technical possibilities to apply such operations. A significant improvement in the properties of steel castings can be obtained through quenching followed by tempering heat treatment, resulting in the formation of the structure of tempered martensite and/or bainite. The mechanical properties of quenched and tempered castings made of low-alloy cast steels characterised by high metallurgical purity and having the structure of tempered martensite and bainite are similar to those of hot-rolled steel products having the pearlitic-ferritic structure [4]. However, not every casting can be subjected to quenching and tempering treatment, e.g. because of the potential formation of cracks and/or deformations during quenching. Therefore, if quenching and tempering treatment is not possible to apply, the normalising heat treatment has to be carried out. Normalising heat treatment refines grains of all phase constituents and decreases interlamellar spacings in pearlite and also changes proportions of contents of the particular phase constituents in the casting. As a consequence of the described microstructure evolution only small changes in hardness and strength can be expected but significant improvement of plasticity and fracture toughness occurs.

In order to obtain high strength and good plasticity comparable with properties attainable after quenching and tempering, a modification of chemical composition of a cast steel is required. Such modification most often involves increasing contents of some alloying elements and improving metallurgical cleanliness. Higher contents of alloying elements could improve mechanical properties when proper normalising parameters are applied but it unavoidably increases interdendritic chemical segregation during solidification. A high chemical segregation does not allow to obtain entirely dual phase pearlitic – ferritic microstructure and in the segregation zones bainite and martensite phases form. Mechanism of fracture of such multiphase heterogenies microstructure of steel casting containing also shrinkage cavities much differs from mechanism of fracture of microscopically homogeneous alloys.

Macroporosity is distributed inhomogeneously within the volume of the casting, causing the local weakening of the product, i.e. the reduction of strength and rigidity. Microporosity is distributed more homogeneously, reducing mechanical parameters uniformly within the volume of the product. In terms of inhomogeneous porosity distribution, related results of research concerning quenched and tempered low-alloy cast steels [5, 6] and corrosion-resistant steel castings [7] revealed that the critical parameter responsible for a decrease in the mechanical and plastic properties of castings was the local highest accumulation of porosity in a loaded element. It was not explicitly determined whether the effect of a smaller number of large pores had the same or a different effect to that of a larger number of smaller pores of the same volume.

The quantitative description of the plastic (ductile) fracture process of a stressed material containing a specific initial volume fraction of cavities and cavity nucleation centres (e.g. non-metallic inclusions) can be perform with the use of constitutive models based on the micromechanism of nucleation, growth and coalescence of existing cavities and cavities formed during deformation. The Gurson-Tvergaard-Needleman model (GTN model) is one the most widely used in this area of fracture analysis [8-13]. Recently Zhang et al. [13] analysed possibilities and limitations of application of GTN model to predict fracture of various alloys. They indicated two main drawbacks which restrict wider applications of the GTN model: lack of possibility to predict accurate results when plastic fracture is caused by shear mechanism and required many model parameters to be determined experimentally. The authors of publication [13] also summarised works concerned with extending the applicability limits of the GTN model, including cases where the strain micromechanism is different from the ductile cavity mechanism in the entire separation area, particularly for a case of the mixed micromechanism including ductile cavity fracture and plastic fracture triggered by the shear mechanism.

There were attempts to develop a model describing the fracture mechanism of ferritic steels in the phase of transition from cavity ductile fracture to cleavage fracture by combining the GTN model with the Beremin model describing the cleavage fracture [14], but the application level of the transition model was not obtained [15]. Developed until now numerical models and experimental correlations between the quantitative characteristics of discontinuities in castings and mechanical properties are not sufficiently precise to be used as normative tools for the design of structures and devices. In particular, it is not possible to calculate the critical dimension and number of shrinkage cavities in specific castings causing decrease in mechanical properties below acceptable minimum. Standard specifications for castings contain acceptance criteria based only on engineering experience. For this reason, it is necessary to adopt higher safety factors for castings in comparison with steel products manufactured using plastic working methods.

The research work presented in this article aimed to identify and discuss the microstructural fracture mechanism of normalising heat treated low-alloy medium-carbon cast steels having the multiphase pearlitic-ferritic structure with fractions of martensite and bainite, under tensile stress conditions. In view of the fact that, until today, no constitutive model enabling the quantitative description of the mixed cleavage-ductile fracture mechanism in presence of voids (as is the case with multiphase cast steels) has been developed, in research work presented in the paper physical investigation methods were used to analyse the fracture mechanism. It is believed that results of this research enlarged microstructural data base required for developing more advanced numerical models describing fracture of multiphase alloys containing voids.

The main novelty of research methodology and results of investigation presented in this work is the attempt to describe at micrometre scale the process of nucleation, coalescence and growth of cracks at presence of shrinkage microcavities in cast steel with multiphase microstructure characterising by heterogenous distribution of phase constituents.

2. Design of the chemical compositions of experimental cast steels and melting and casting of the designed cast steels

The contents of chemical elements in the experimental cast steels intended for normalisation heat treatment were designed on the basis of the analysis of experimental data concerning the

effect of alloying elements content on the phase composition of the cast steel. The correlations between mechanical properties and parameters characterising the pearlitic-ferritic microstructure were also taken into account [16, 17].

The objective was to obtain the following mechanical properties in the normalised state: ultimate tensile strength UTS or R_m[1] > 550 MPa, yield strength YS or $R_{p0.2}$ > 400 MPa, percentage total elongation at fracture EL or A> 5% and the fulfilment of weldability condition: $C_E \leq 0.6$[2], where

$$C_E = \%C+\%Mn/6+(\%Cr+\%Mo+\%V)/5+(\%Ni+\%Cu)/15 \quad (1)$$

The research work involved the design of the chemical compositions of four experimental cast steels constituting the basis for determining the target chemical composition satisfying the assumed (as shown above) mechanical properties. Chemical compositions of the designed experimental cast steels have no equivalent grades in the standards.

Laboratory melts were prepared using slag-less process in a VIM-LAB30-75 vacuum induction furnace with a crucible made of a magnesite mixture containing (in dry state), in mass %: MgO - 88.7 %; Al_2O_3 - 3.5 %; SiO_2 - 3.8 %; CaO - 3.8 % and Fe_2O_3 - 0.2 %. All the experimental melts marked SC1, SC2, SC3 and SC4 were made using pure metallic and non-metallic components: Mn, Cr, Al, Si, C, ferroalloy FeV and high purity Armco. Sand applied for preparing the moulds contained, in mass %: SiO_2 - 98.4 %; Fe_2O_3 - 0.18 % and bentonite as the binder. The metal in the furnace crucible before casting weighed approximately 20 kg. Each melt was cast gravitationally in an air atmosphere (after opening the furnace), into a sand mould made so that a casting consisting of two parallel plates having dimensions of 400 mm x 135 mm x 15 mm (Fig. 1a,b) could be obtained. Time of pouring the moulds ranged from 8 seconds to 10 seconds. The chemical compositions of the test cast steels, determined using the OES method and a Magellan Q8 spark emission spectrometer (Bruker) are presented in Table 1.

a)

b)

Fig. 1. a, b. Photographs of experimental steel castings after cutting off risers

Table 1.
Results of analyses concerning the chemical compositions of experimental cast specimens, wt %, *exceptions: O and N in ppm, n.a. – not analysed; C_E – carbon equivalent, To [°C] - pouring temperature (measured temperature of the liquid metal directly before pouring)

	SC1	SC2	SC3	SC4
C	0.24	0.35	0.28	0.31
Mn	1.21	1.60	1.43	0.87
Cr	0.0	0.0	0.0	0.42
Si	0.63	0.60	0.57	0.58
P	0.003	0.004	0.004	0.003
S	0.006	0.006	0.005	0.005
Al	0.014	0.024	0.016	0.017
V	0.00	0.00	0.10	0.10
O*	n.a.	6	17	n.a
N*	n.a.	< 20	< 20	n.a.
C_E	0.44	0.62	0.55	0.56
To	1546	1550	1544	1544

3. Research methodology

3.1. Microstructural investigation

The microstructure of the specimens sampled from the experimental castings in the solidified state and after the application of heat treatment variants was observed and imaged on unetched and etched metallographic specimens using a DSX500 digital light microscope OLYMPUS (LM) and an Inspect F scanning electron microscope - FEI (SEM). The identification of the microstructure of the specimens subjected to LM and SEM observations required the etching of the specimens using the HNO_3 solution in ethanol, i.e. Nital reagent. Macroporosity and other macrodiscontinuities were observed on the unetched and etched cross-sectional surfaces of the specimens using magnifications of up to 35x.

[1] Symbols representing parameters of mechanical properties follow the requirements of international standard: EN ISO 6892-1: Metallic materials - Tensile testing - Part 1: *Method of test at room temperature*

[2] Chemical element contents in the formula for calculating C_E, as well as in the entire article, are expressed in wt%

3.2. Identification of specimen porosity based on density measurements

The porosity of the specimens was determined by means of density measurements performed using the hydrostatic weighing method (Archimedes' method) [18,19]. The density measurements involved specimens having dimensions of 55 mm x 10 mm x 10 mm, cut out of the plates in the as-cast state and specimens sampled from the castings subjected to hot pressing deformation (in order to eliminate or significantly reduce porosity), having dimensions of 50 mm x 25 mm x 5 mm. Based on the experimental data concerning the critical amount of deformation closing porosity entirely [20, 21], the parameters adopted for the hot pressing of the test plate sections were: deformation temperature within the range of 1150°C to 1000°C and a total amount of deformation of 45%. During hot pressing the applied force was not measured directly, but it was calculated using parameters of forging and yield stress at forging temperature measured during earlier experiments of hot pressing of similar class of alloys, carried out using Gleeble simulator. The mean yield stress measured for temperature range of 1150 - 1000°C was 150 MPa and calculated maximum force applied during hot pressing of the investigated in this work specimens is equal to 188 kN.

3.3. Measurement of mechanical properties

The specimens designed to tensile tests were cut out from the cast plates subjected to selected heat treatment variants. Locations of tensile specimens on surface of the plate are shown in Figure 2.

The tensile tests, performed using a Z250 testing machine (Zwick/Roell), were carried out on flat specimens having cross-sectional dimensions of 8 mm × 15 mm and a gauge length of 80 mm. A low strain rate of $4.0 \cdot 10^{-3} s^{-1}$ was applied, characteristic of quasi-static tension. Elongation measurements, performed using an extensometer, involved the middle section of the specimen. The value of the strain rate was the same in relation to all the test specimens. The tensile tests, performed in accordance with the PN-EN ISO 6892-1:2020-05 standard, resulted in the determination of offset yield strength $R_{p0.2}$, tensile strength R_m and percentage total extension at fracture A_5. Hardness measurements were performed using the Brinell method on the surface of cross section of the plates in the as-cast and normalising heat treated states. Locations of points for hardness measurement are indicated in Figure 2.

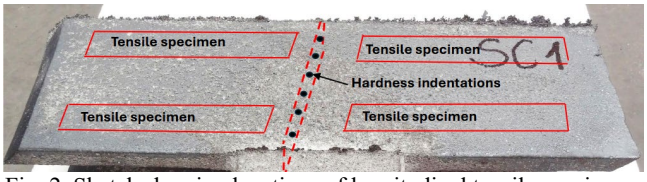

Fig. 2. Sketch showing locations of longitudinal tensile specimens on surface of the cast plate and points of hardness measurements on transverse cross section of the plate

4. Results

4.1. Macrostructure, microstructure and the hardness of the experimental cast steels in the as-cast state

The unetched metallographic specimens sampled from the cast plates were observed for the presence of cavities, discontinuities and non-metallic inclusions using SEM. Because of high purity of the investigated castings only small number of very fine particles of non-metallic inclusions were found. SEM observation and microanalysis by EDS method revealed that the fine non-metallic inclusions were manganese sulphides and complex oxy-sulphides. The maximum linear size of cavities or porosity in investigated cross-sections was within the approximate range of 1 mm to 2 mm (example in Fig. 3a,b). The cavities observed on the metallographic specimens only represented the examined cross-sections of the cast plates and, for this reason, did not characterise the porosity of the entire casting. The dendritic morphology of the internal surfaces of the cavities indicated that the cavities were formed in the interdendritic areas at the last stage of the steel solidification process, as a result of the shrinkage of the cast steel and the lack of the liquid phase. The test surfaces did not contain any cracks. The comparison of LM images concerning the pearlitic-ferritic microstructure of the test castings revealed differences in the distribution of ferrite grains against the pearlitic structure (background). In plates from heats SC1 and SC2, ferrite grains precipitated primarily at the boundaries of large grains of primary austenite (example in Fig. 4a), whereas the distribution of ferrite grains in plates from heats SC3 and SC4 was more homogenous (example in Fig. 4b). The aforesaid difference resulted from various sizes of primary austenite grains, dependent on the mechanism of steel solidification. The SEM-based observations revealed that all the test castings contained the pearlitic-ferritic microstructure. The pearlitic-ferritic microstructure consisted of pearlite colonies, characterised by varied morphology (dependent on the form of cementite particles, i.e. lamellar, degenerated and divorced (globular)) [22-25] as well as of ferrite phase in form of grains, lamellae and other shapes of various sizes, variedly distributed in the cast steel matrix. In the as-cast state, no microstructural constituents other than pearlite and ferrite were observed. In particular, no martensite was detected. The hardness measurements of the plates in the as-cast state were performed on the cross-sectional surface using the Brinell HBW 5/750 method. Because the melting and casting parameters as well as the shape and dimensions of the castings were identical in relation to all four cast steels, the differences in the hardness of the castings resulted from the effect of the chemical composition of a given cast steel on the microstructure. The lowest hardness (within the range of 161 HBW to 169 HBW) was observed in the plates made of cast steel SC1. Cast steel SC2 was characterised by hardness approximately 30 HBW higher (within the range of 185 HBW to 207 HBW) than that of SC1. The highest hardness was observed in cast steel SC3 (within the range of 193 HBW to 209 HBW) and SC4 (within the range of 191 HBW to 204 HBW).

a) b)

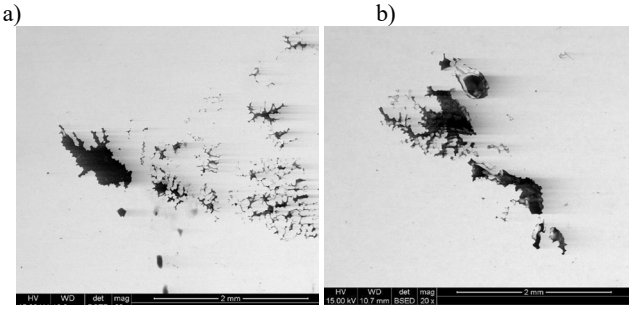

Fig. 3a, b. Exemplary SEM images of maximally-sized cavities observed on the unetched metallographic specimens sampled from the following cast plates: (a) plate from heat SC2 and (b) plate from heat SC3

a) b)

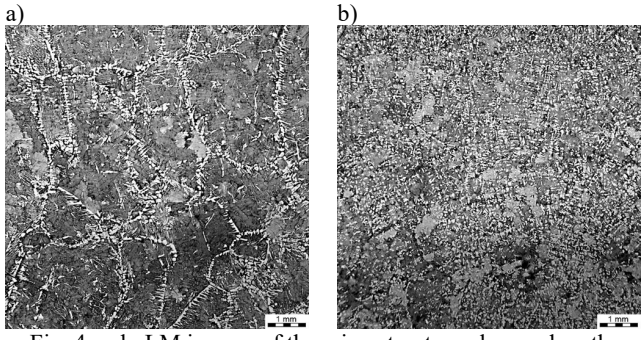

Fig. 4. a, b. LM images of the microstructure observed on the etched metallographic specimens sampled from the cast plates: (a) heat SC1 and (b) heat SC3

4.2. Density-measurement-based assessment of porosity of the castings

The porosity of the specimens sampled from the experimental castings was calculated by means of formula (2), based on specimen density values measured at ambient temperature using the hydrostatic weighing method (Archimedes' method):

$$P_o\ [\%] = (1 - \rho_o / \rho_p) \cdot 100 \qquad (2)$$

where P_o - casting porosity, i.e. porosity of the casting identified in relation to the condensed state obtained using the plastic working method (in vol% or wt%), ρ_o - casting density and ρ_p - density measured after the hot plastic working of the casting.

Each cast steel, i.e. SC1, SC2, SC3 and SC4, was subjected to density measurements involving eight specimens sampled from the test plates in the as-cast state. The ranges of measured porosity values of individual specimens and the mean porosity values of the plates cast from experimental cast steels were the following:

- cast steel SC1 - results of individual measurements were within the range of 0.19% to 0.95%, whereas the mean value amounted to 0.61%;
- cast steel SC2 - results of individual measurements were within the range of 0.52% to 2.37%, whereas the mean value amounted to 1.18%;
- cast steel SC3 - results of individual measurements were within the range of 0.15% to 0.88%, whereas the mean value amounted to 0.52%;
- cast steel SC4 - results of individual measurements were within the range of 0.12% to 1.11%, whereas the mean value amounted to 0.54%.

The presented values revealed that the porosity of the test plates obtained from cast steels SC1, SC3 and SC4 were similar, whereas the porosity of the plates made of cast steel SC2 was approximately twice as high. The twofold increase in the value of porosity of the plates made of cast steel SC2 could be attributed to the higher contents of carbon and manganese (affecting the mechanism of solidification) in comparison with those in cast steels SC1, SC3 and SC4 (Tab. 1). Increased contents of carbon and manganese led to the formation of more austenite and less ferrite in the first solidified phase. The increased content of austenite, characterised by higher density compared to that of ferrite, triggered greater shrinkage in the solidified phase and could be responsible for an increase in the volume of shrinkage cavities.

4.3. Microstructure and mechanical properties of experimental cast steels after normalising heat treatment

The austenitising temperature used within the process of normalising heat treatment was determined on the basis of calculated values of temperature A_{c3} in relation to the chemical composition, using the empirical formula presented in [26,27]. The adopted austenitising temperature was 900°C and time of holding at the austenitising temperature amounted to 30 minutes. The cooling of experimental plates after austenitising was performed in two variants: in still air – causing cooling of the mid-area of the plate in the temperature range 900-500°C at rate of 1.5°C/s and in air stream blown by a fan at a flow rate of 5 m/s - causing cooling of the mid-area of the plate in the temperature range 900-500°C at rate of 2.5°C/s. The performance of single normalising was followed by the determination of the effect of double normalising, which (according to the information contained in reference publication [28]) could favourably affect the refinement of microstructure and mechanical properties. Because of the refinement of austenite grains resulting from the austenitising of the castings, ferrite grains formed at austenite grain boundaries depicted dendrite axes, being the areas of segregation characterised by reduced contents of chemical elements in relation to the mean contents of elements in the cast steel. In Figures 5a,b examples of typical dendritic microstructure of the investigated plates are presented. The darkest areas and spots represent shrinkage cavities developed during solidification whilst the lightest pattern represents axes of the dendrites.

a) b)

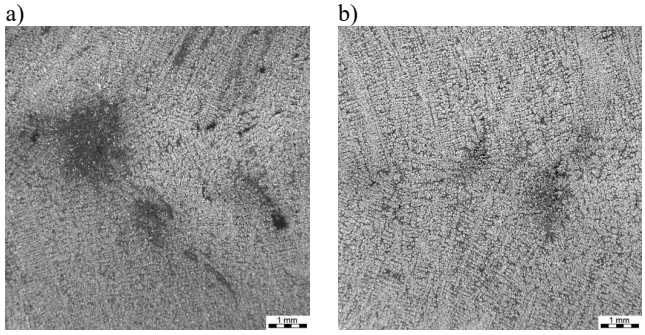

Fig. 5a,b. LM images of the macrostructure observed on the etched metallographic specimens sampled from the normalised plates subjected to austenitising at a temperature of 900°C for 30 minutes, followed by cooling in still air: (a) cast steel SC2 and (b) cast steel SC3

The refinement of pearlite and ferrite grains as well as interlamellar spacings in pearlite resulting from the performance of the normalisation process are presented in Figures 6a,b as SEM microphotographs. The normalised castings made of SC1 and SC4 cast steels were characterised by the pearlitic-ferritic microstructure including lamellar pearlite and degenerated pearlite containing cementite precipitates of irregular and varied shapes. The normalised castings made of cast steels SC2 and SC3 contained two types of microstructure, i.e. the quantitatively dominant areas of pearlitic-ferritic structure with pearlite of diversified cementite morphology as well as zones formed in the interdendritic areas, containing pearlite, ferrite and, in addition, martensite and bainite (Fig. 7a,b).

a) b)

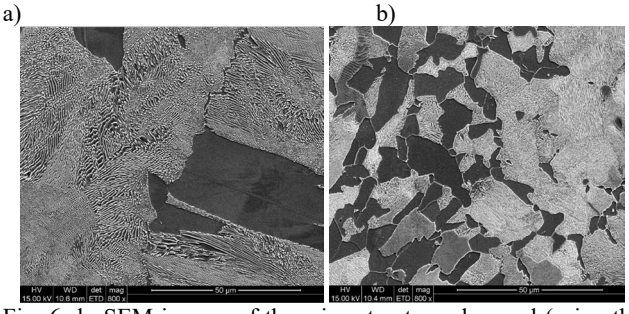

Fig. 6a,b. SEM images of the microstructure observed (using the same magnification) on the etched metallographic specimens sampled from the plate made of cast steel SC2: (a) in the as-cast state and (b) after normalising with cooling in still air

a)

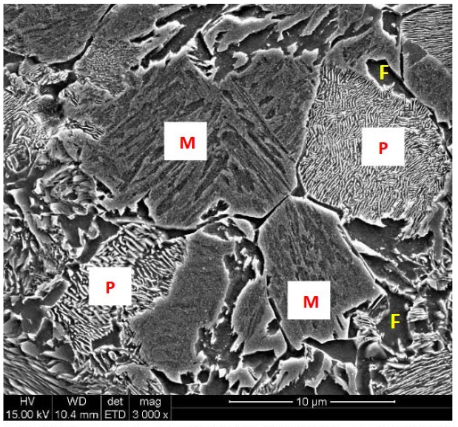

b)

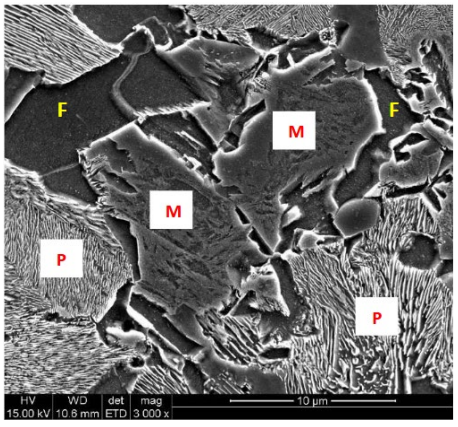

Fig. 7a,b. SEM images of the microstructure observed in the interdendritic spaces on the etched metallographic specimens sampled from the normalised plates subjected to austenitising at a temperature of 900°C for 30 minutes, followed by cooling in still air: (a) cast steel SC2 and (b) cast steel SC3; P – pearlite, F – ferrite, M – martensite

The heat treatment variants used in the tests significantly modified the microstructure of the castings, yet the hardness values of the plates after normalising did not differ considerably from those plates in the as-cast state. The foregoing resulted from the opposing effects of two mechanisms. On one hand, heat treatment was responsible for the significant refinement of austenite grains and, consequently, the refinement of grains in the final structure, which led to increased hardness. However, on the other hand, austenite grain refinement led to an increase in the fraction of the ferritic phase at the expense of the pearlitic phase, which led to a decrease in hardness. The use of heat treatment leading to grain refinement aimed at improving the plastic properties of the castings. It was also found that the use of double normalisation did not trigger any significant changes in the microstructure and hardness if compared to one-time normalisation, which constituted the basis for selecting the treatment variants including single normalisation in the subsequent tests. From each test plate subjected to the selected variant of heat treatment two specimens for the tensile test were prepared. The results of tensile tests are presented in Table 2. For the optimum chemical composition and normalising parameters of the experimental cast steels yield strength reached 407-440 MPa,

tensile strength attained 586-601 MPa and elongation was 6-8%, which values are higher than properties of standard grades of structural cast steels in normalised condition. The SEM observations of the morphology of the rupture surface involved those variants of the chemical composition and heat treatment of the cast steels which were characterised by multiphase microstructure composed of P+F matrix constituents and M+B bands. The multiphase variants showed the most favourable values of parameters $R_{p0.2}$, R_m and A_5, i.e.: variant 21P (specimens 21P-1 and 21P-2) – items 5 and 6 in Table 2 and variant 31P (specimens 31P-1 and 31P-2) – items 9 and 10 in Table 2. The rupture surface contained areas formed as a result of the fracture of the material not containing cavities and porosity (Fig. 8a,b) as well as areas with visible internal surfaces of shrinkage cavities having the dendritic structure (Fig. 9a,b). The rupture surface in the areas not containing cavities was of highly developed cleavage-ductile nature, with small-sized cleavage facets.

Table 2.
Tensile test results of the flat specimens made of the normalised cast steel plates cooled form austenitising temperature in still air (P) or cooled faster in air stream (N)

Cast steel	No.	Specimen	$R_{p\,0.2}$, MPa	R_m, MPa	A_5, %
SC1	1	11P-1	341	551	14.0
	2	11P-2	356	585	20.0
	3	11N-1	344	523	12.2
	4	11N-2	355	584	18.7
SC2	5	21P-1	407	601	7.3
	6	21P-2	420	716	22.0
	7	21N-1	408	609	6.2
	8	21N-2	411	596	7.0
SC3	9	31P-1	454	553	5.8
	10	31P-2	440	586	8.8
	11	31N-1	451	591	7.0
	12	31N-2	434	461	4.5
SC4	13	41P-1	400	492	6.5
	14	41P-2	364	373	5.7
	15	41N-1	371	408	4.7
	16	41N-2	418	580	9.5

a) b)

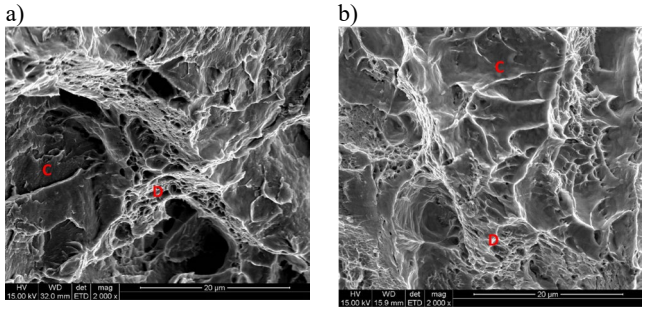

Fig. 8. a, b. Fractography images of the specimen rupture surface, subjected to uniaxial tensile tests: (a) specimen 21P-1 and (b) specimen 31P-2; D – ductile-cavity fracture and C – brittle-cleavage fracture

a) b)

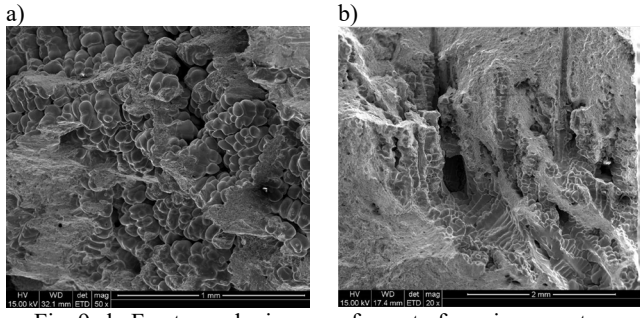

Fig. 9a,b. Fractography images of a part of specimen rupture surface, subjected to uniaxial tensile tests – areas containing the internal surface of the shrinkage cavity: (a) specimen 21P-1 and (b) specimen 31P-2

4.4. Microstructural fracture mechanism under tensile stress

For investigation of the microstructural fracture mechanism under tensile stress the normalised castings with multiphase microstructure consisting of the pearlitic-ferritic matrix and martensitic-bainitic bands were used. Multiphase microstructure with inhomogeneously distributed bands of martensite and bainite was produced in normalised castings SC2 and SC3, whereas in castings SC1 and SC4 fully pearlitic-ferritic microstructure formed. Therefore, the microstructural fracture mechanism was investigated using the tensile fractured specimens made from castings SC2 and SC3, designated as 21P-1, 21P-2, 31P-1 and 31P-2 – items 5, 6, 9 and 10 in Table 2. The microstructural observations involved the surface of the longitudinal cross-section of the ruptured specimens in the area directly under the rupture surface and in the areas distant from the rupture surface within the specimen area reduction. The normalising heat treatment of the castings made of cast steels SC2 (specimens 21P-1 and 21P-2) and SC3 (specimens 31P-1 and 31P-2) led to the formation of microstructure consisting of quantitatively dominant areas having the pearlitic-ferritic structure and zones formed in the interdendritic areas characterised by increased contents of alloying elements (in relation to the mean content in the cast steel) and containing martensite and bainite (zones M+B). It was found that, during the uniaxial tensile test, the nucleation of cracks in the multiphase-structured cast steel took place primarily at the pearlite-ferrite interfaces (Fig. 10a), at the ferrite-ferrite grain boundaries (Fig. 10b), within the pearlite colony (Fig. 10c) as well as at the martensite-martensite interfaces and transversely across the martensite and bainite lath packets (Fig. 10d). No any noticeable influence of the fine non-metallic inclusions present in the castings on the mechanism of crack initiation and development of fracture was detected.

In relation to the linear size, the cavities present in the test specimens were divided into microcavities (having a size of up to 50 μm), mesocavities (of intermediate size; having a linear size within the range of 50 μm to 500 μm) and macrocavities (having a size in excess of 0.5 mm). The micro and mesocavities were formed primarily in the interdendritic segregation zones and, for that reason, were surrounded by a matrix containing martensite

and bainite, characterised by lower plasticity than that of the matrix.

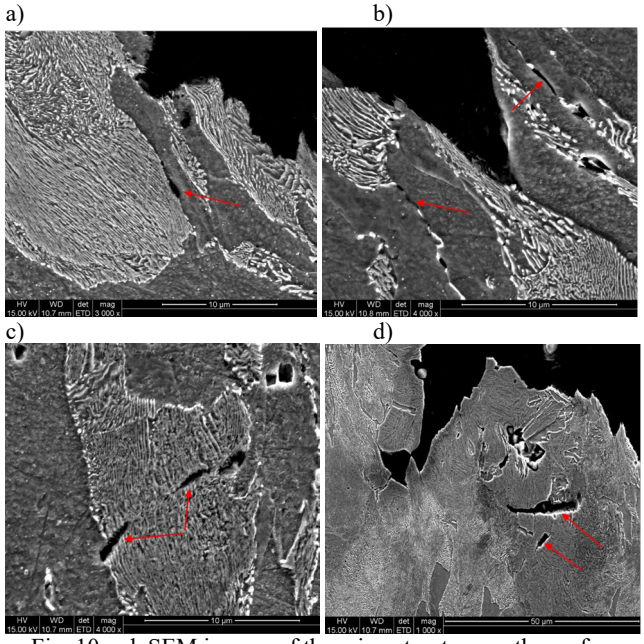

Fig. 10 a-d. SEM images of the microstructure on the surface parallel to the tensile axis, presenting typical cracks nucleation centres: (a) crack at the P-F interface, specimen 21P-1, (b) cracks at the ferrite grain boundary, specimen 21P-1, (c) cracks within the pearlite colony, specimen 31P-1 and (d) cracks at the martensite grain boundary and across the martensite lath packets, specimen 21P-2

The tensile test led to the non-uniform distribution of plastic strain, where the pearlitic-ferritic matrix was deformed to a greater extent, whereas the M+B zones underwent lesser deformation. Because of the low plastic strain of the M+B zones, the material around the micro and mesocavities in the above-named zones underwent a smaller plastic strain than that observed in the pearlitic-ferritic matrix. As a result, the microcavities in the M+B zones did not undergo coalescence. In addition, the M+B zones did not undergo a significant plastic strain in the area directly under the rapture surface either, where fracture took place along the grain boundaries and the cleavage facets in the lath packets in martensite and bainite (Fig. 11a). Shrinkage micro and mesocavities were also present in the P+F matrix, yet their amounts were smaller than those in the M+B zones. The P+F matrix areas underwent a significant plastic strain, with cracking taking place along with the formation of the dimple-cleavage fracture surface (Fig. 11b). The dimple-type morphology of the rupture surface was formed primarily in the ferritic areas, whereas the cleavage-type morphology was formed mainly in the pearlitic areas. When the microcavities in the P+F matrix were separated by large distances, which was often the case in the test specimens (Fig. 12a), they did not undergo coalescence during the plastic strain. The bridges between micro and mesocavities located near one another in the P+F matrix fractured directly under the rupture surface and joined the newly formed cracks, thus leading to the rupture of the specimen (Fig. 12b).

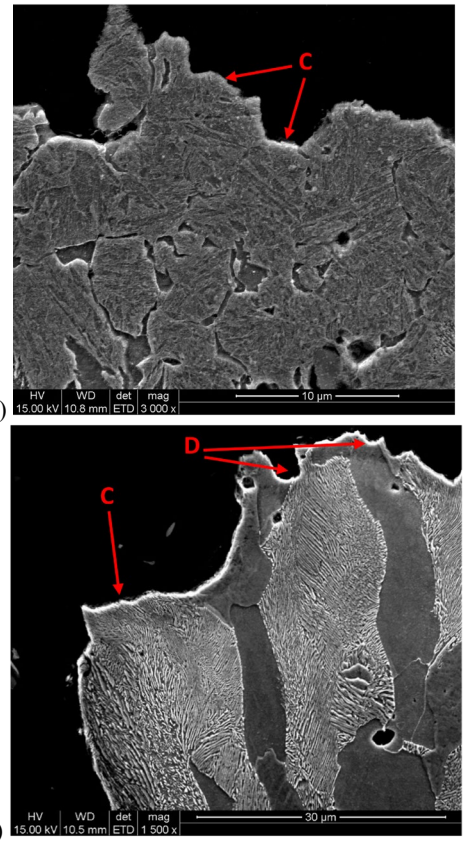

Fig. 11 a,b. SEM images of the cross-section under the test specimen rupture surface: (a) martensitic zone in specimen 31P-1 and (b) pearlitic-ferritic zone in specimen 31P-2; C – cleavage-brittle fracture and D – dimple-ductile fracture

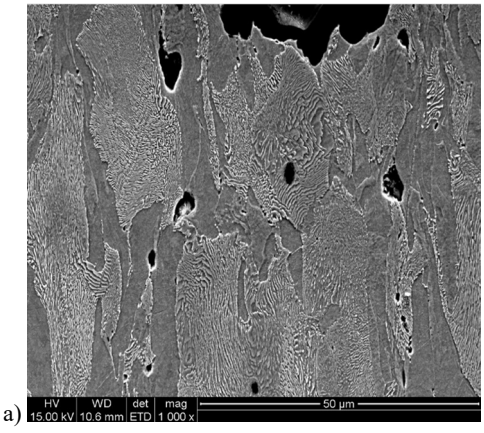

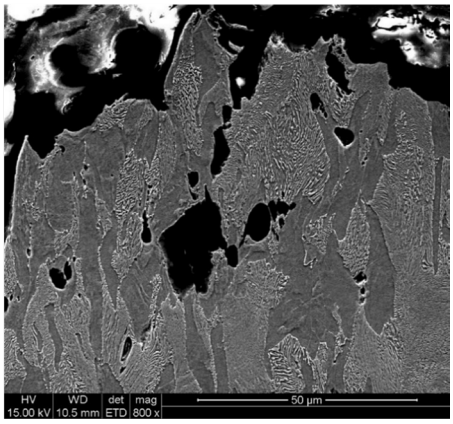

b)

Fig. 12a,b. SEM images of specimen 21P-2 directly under the rupture surface: (a) single shrinkage microcavities in the P+F matrix, (b) cracking of bridges (coalescence) between the microcavities located near one another and newly-formed cracks

5. Discussion

5.1. Heat-treatment-based modification of the microstructure of experimental castings

The improvement of the mechanical properties and stress relief of the castings required to carry out the normalising heat treatment, leading to the refinement of ferrite grains and pearlite colonies as well as the reduction of interlamellar spacings in pearlite. The faster cooling of the normalised castings from the austenitising temperature in relation to cooling in the casting mould resulted in the formation of martensite and bainite in the zones of the interdendritic segregation of chemical elements in castings SC2 and SC3. In the segregation zones of cast steels SC1 and SC4, it was possible to observe the pearlitic-ferritic structure characterised by a greater amount of pearlite and finer ferrite grains than those observed in the remaining part of the matrix. It should be noted that in low-alloy carbon-manganese steels having a carbon content of more than approximately 0.25% and a manganese content of more than approximately 1.4%, the interdendritic segregation of manganese during solidification inevitably leads to the formation of zones characterised by higher hardenability. As a result of cooling from the austenitising temperature at a rate higher than the critical value, part of austenite in the segregation zones transforms into bainite and martensite. Designing the chemical composition of normalised cast steels having improved properties if compared to standard cast steels used in normalised condition should take into account the effect of the interdendritic segregation of alloying elements on phase transformations and the final microstructure and properties. For example the segregation coefficient of Mn can range between 1.1 and 2.6 depending on chemical composition and conditions of cooling of solidifying melt [29,30] and the effect of such segregation is significant inhomogeneity of microstructure in the volume of the casting.

5.2. Morphology of the rupture surface of tensile test specimens

The rupture surface of the tensile test specimens in the areas not including cavities was characterized by mixed cleavage-ductile morphology, with small-sized cleavage facets. In the areas containing shrinkage cavities, the internal surfaces of raptured cavities were characterised by dendritic morphology. The analysis concerning the correlation between the shape of the rupture surface and the microstructure observed on the plane perpendicular to the rupture surface revealed that the cleavage planes were located primarily across the pearlite colonies and, in the segregation zones, across the packets of martensite and bainite laths. The identified mode of fracture of pearlite colonies in the investigated cast steels is the same as fracture mode in fully pearlitic steels [31] and fracture mode observed in bainitic and martensitic zones is the same as in fully bainitic or fully martensitic steels [32]. In ferrite areas the dimple-type morphology of the rupture surface was observed as is typical for soft phase constituent.

5.3. Heat-treatment-based modification of the microstructure of experimental castings

The mechanical properties of cast steels depend on microstructural parameters, contents of alloying and residual elements and also on morphology, distribution in volume, sizes and types of material discontinuities, including shrinkage cavities. The identification of the quantitative effect of the volume fraction as well as the distribution and sizes of cavities on mechanical properties can be performed on the basis of tests of steel castings having the same or similar chemical compositions, cast and heat-treated under identical conditions. To develop a quantitative relationship characterised by a high correlation coefficient a large amount of experimental data is required, which were not available for the experimental cast steels investigated within the present research work. For this reason, it was possible to formulate only qualitative conclusions regarding the effect of microstructure, shrinkage voids and dendritic inhomogeneity on mechanical properties of the investigated castings.

The results of the tensile tests revealed that, for the specimen from the same casting and subjected to the same heat treatment, a larger total fraction of cavities on the rupture surface corresponded to lower values of ultimate elongation, yield strength and tensile strength. It should be emphasized that the sizes and shapes of the cavities observed on the rupture surfaces were not the same cavities which were formed during solidification and cooling as the plastic strain was accompanied by the deformation and coalescence of the original cavities. Gradual changes of shapes and dimensions of the shrinkage cavities and their coalescence caused by plastic deformation were observed on longitudinal cross-sections of tensile specimens, as shown in Figures 12a,b. Evolution of shapes of the cavities with the increase of plastic strain was revealed by investigation of various places in tensile specimens – from undeformed grip part, to fractured surface.

The values of reduced mechanical parameters identified on the basis of measurement results concerning the particular specimens cut out of the casting did not characterise the entire volume of the casting, but only its part subjected to the test. The identification of the critical size or volume of a single cavity, a cluster of adjacent cavities or all cavities present in the loaded part of the casting, reducing the mechanical properties below a demanded minimum requires further research. Further work is needed regarding quantitative metallographic description of bulk microstructure and discontinuities existing before loading and the changes identified in microstructure after fracture. A final purpose is to develop a correlation between mechanical properties and microstructural parameters of cast steel with multiphase microstructure containing shrinkage cavities. Such quantitative correlations have been developed for steels produced with the use of hot working after casting (example [16]).

5.4. Microstructural fracture mechanism

Depending on the contents of carbon and alloying elements, a pearlitic-ferritic microstructure or a multiphase microstructure is formed in normalised thin and medium-walled steel castings. In addition to pearlite and ferrite, the above-named multiphase structure also contains areas of martensite and bainite. Under stress conditions, in a material having a two-phase or multiphase structure, the distribution of plastic strain is inhomogeneous, where the deformation of phases having a lower yield strength is greater. In terms of the phase constituents under analysis, the order of susceptibility to plastic strain (from the highest to the lowest) is as follows: ferrite, pearlite, bainite and martensite. During the uniaxial tensile test, the nucleation of cracks in the multiphase cast steels took place primarily at the pearlite-ferrite interfaces, at the ferrite-ferrite grain boundaries, within pearlite colonies, at the boundaries between martensite grains and between bainite grains as well as across the martensite and bainite lath packets. In the pearlitic-ferritic matrix (P+F), shrinkage cavities separated by large distances did not undergo coalescence during the plastic strain. The bridges between the micro and mesocavities located close to one another in the P+F matrix fractured directly under the rupture surface. The fracture in the areas having the P+F microstructure took place through the coalescence of newly formed cracks and existing cavities producing the dimple-cleavage fracture. The dimple-type morphology was formed primarily in the ferritic areas, whereas the cleavage-type morphology was formed mainly in the pearlitic areas. Because of the low plastic strain of the zones containing martensite and bainite (M+B zones), the material around the micro and mesocavities in the aforesaid zones underwent a smaller plastic strain than the pearlitic-ferritic matrix. As a result, no coalescence of the microcavities in the M+B zones was observed. In the M+B zones, cracks propagated directly under the rupture surface through the growth and coalescence of newly formed cracks. The shrinkage macrocavities reduced the load-bearing capacity of the loaded element mainly because of reduction of the cross-sectional area transferring the load.

Because of the complex microstructural fracture mechanism operating in steel castings having multiphase inhomogeneous microstructure containing microcavities, the quantitative description of their deformation and fracture could not be performed using models developed for the conditions of homogeneous ductile fracture, such as the GTN model or existing modifications of the GTN model [8-13]. An attempt to develop a combined plastic-cleavage model was proposed in study [33], where it was used to describe the deformation and failure behaviour of dual-phase steel grades (DP) and steel grades characterised by transformation-induced plasticity (TRIP) having multiphase microstructure. A model proposed in work [33] contained a two-term description, including the GTN model used to simulate plastic fracture in the ferritic phase and a cohesive zone model (CZM) to simulate cleavage fracture along the martensite-ferrite interfaces. Investigated multiphase microstructure was modelled in [33] using a method of the representative volume elements (RVE). Tensile tests and hydraulic bulge tests of the investigated DP and TRIP steels were carried out at room temperature to obtain the stress-strain relationships to verify the numerical simulations. Experimental results showed acceptable accuracy of the model predictions concerning formability in the stretch-forming test as well as in the hole expanding test. In work [34] a combined GTN-CZM model was developed for modelling fracture of hydrogen embrittled steel. The ductile-to-brittle transition (DBT) phenomenon was considered as the competition between the fracture in a brittle way - simulated with CZM model, and the fracture in a ductile way - simulated with GTN model.

To adapt the combined cleavage-ductile fracture model (described for example in works [33] and [34]) for simulation of deformation and failure mechanisms operating in multiphase cast steel, the effect of inhomogeneous distribution of phase constituents following the dendrite pattern and shrinkage cavities should be additionally included.

6. Conclusions

1. The shrinkage cavities observed on the cross-sections of the four experimental low-alloy cast steels were characterised by linear dimensions ranging from several dozen micrometres to approximately 2.0 mm. The mean relative volumes of cavities determined for the investigated specimens were in the range of 0.52-1.18%.
2. As a result of normalising heat treatment, the microstructure formed in the test plates was characterised by the significantly smaller grain size of phase constituents than those observed in the plates in the as-cast state. The microstructure consisted of ferrite grains and areas containing pearlite colonies and, in cases of certain variants of chemical compositions, zones containing martensite and bainite.
3. The results of tensile tests of the heat treated castings revealed that the greater fraction of cavity areas on the rupture surface corresponded to the lower values of ultimate elongation, yield point and tensile strength. The rupture surface in the areas not containing cavities was characterised by mixed cleavage-ductile morphology.
4. A detailed microstructural investigation of nucleation, coalescence and growth of cracks at presence of shrinkage microcavities allowed to gain a new insight into fracture

mechanism of multiphase heterogenous cast steel. Fracture propagation in the areas having the pearlitic-ferritic microstructure took place through the coalescence of newly formed cracks and existing shrinkage cavities leading to the formation of dimple-cleavage morphology of fracture surface. In the martensitic-bainitic areas, cleavage transgranular and intergranular cracks propagated directly under the rupture surface as a result of growth and coalescence of the crack nuclei.

5. Suggested directions of future investigations of steel castings with multiphase microstructure should involve development of methodology to determine the critical size and critical volume of cavities reducing the mechanical properties of the castings below the acceptable minimum. Achievement of this aim would be facilitated by availability a numerical failure model allowing for operation of the identified in this work microstructural fracture mechanisms in multiphase inhomogeneous microstructure containing cavities.

Acknowledgements

The results of investigation presented in the article were performed within research work no. S0B063/2024/GIT-Łukasiewicz Research Network - Upper Silesian Institute of Technology, financed from a statutory grant funded by the Ministry of Science and Higher Education of Poland.

References

[1] Garbarz, B. (2018). Structure of continuously cast ingots of unalloyed and low alloy steels and its evolution as a result of hot working. *Prace Instytutu Metalurgii Żelaza.* 70(4), 2-23. (in Polish).

[2] Mahomed, N. (2020). Shrinkage porosity in steel sand castings: formation, classification and inspection. In Z. Abdallah, N. Aldoumani (Eds.), *Casting Processes and Modelling of Metallic Materials* (pp. 133-151). DOI: 10.5772/intechopen.94392.

[3] Kostryzhev, A.G., Morales-Cruz, E.U., Zuno-Silva, J., Cardoso-Legorreta E., Ruiz-Lopez I. & Pereloma, E.V. (2017). Vanadium Microalloyed 0.25 C Cast Steels Showing As-Forged Levels of Strength and Ductility. *Steel Research International.* 83(3), 1600166, 1-11. https://doi.org/10.1002/srin.201600166.

[4] Herion, S., de Oliveira, J.C., Packer, J.A., Christopoulos, C. & Gray, M.G. (2010). Castings in tubular structures – the state of the art. *Structures and Buildings.* 163(6), 403-415. https://doi.org/10.1680/stbu.2010.163.6.403.

[5] Hardin, R.A. & Beckermann, C. (2012). Integrated design of castings: effect of porosity on mechanical performance. *IOP Conference Series: Materials Science and Engineering*. 33(1), 012069, 1-8. DOI: 10.1088/1757-899X/33/1/012069.

[6] Hardin, R.A. & Beckermann C. (2013). Effect of porosity on deformation, damage, and fracture of cast steel. *Metallurgical and Materials Transactions A.* 44(12), 5316-5332. https://doi.org/10.1007/s11661-013-1669-z.

[7] Susan, D.F., Crenshaw, T.B. & J. S. Gearhart, J.S. (2015). The effects of casting porosity on the tensile behavior of investment cast 17-4PH stainless steel. *Journal of Materials Engineering and Performance*. 24, 2917-2924. https://doi.org/10.1007/s11665-015-1594-y.

[8] Besson, J. (2010). Continuum models of ductile fracture - A review. *International Journal of Damage Mechanics*. 19(1), 3-52. https://doi.org/10.1177/1056789509103482.

[9] Yan, H., Jin, H. & Yao, R. (2020). Prediction of the damage and fracture of cast steel containing pores. *International Journal of Damage Mechanics*. 29(1), 166-183. https://doi.org/10.1177/1056789519872000.

[10] Wcislik, W. (2016). Experimental determination of critical void volume fraction f_F for the Gurson Tvergaard Needleman (GTN) model. *Procedia Structural Integrity*. 2, 1676-1683. https://doi.org/10.1016/j.prostr.2016.06.212.

[11] Lachowski, J. & Borowiecka-Jamrozek, J. (2021). Analysis of fracture mechanism of cast steel for different states of stress. *Archives of Foundry Engineering*. 21(2), 29-34. DOI: 10.24425/afe.2021.136094.

[12] Kossakowski, P.G. (2017). Experimental determination of the void volume fraction for S235JR steel at failure in the range of high stress triaxialities. *Archives of Metallurgy and Materials.* 62(1), 167-172. DOI: 10.1515/amm-2017-0023.

[13] Zhang, Y., Zheng, J., Shen, F., Li, D., Münstermann, S., Han, W., Huang, S. & Li, T. (2023). Ductile fracture prediction of HPDC aluminum alloy based on a shear-modified GTN damage model. *Engineering Fracture Mechanics*. 291, 109541, 1-21. https://doi.org/10.1016/j.engfracmech.2023.109541.

[14] Bernauer, G., Brocks, W. & Schmitt, W. (1999). Modifications of the Beremin model for cleavage fracture in the transition region of a ferritic steel. *Engineering Fracture Mechanics*. 64(3), 305-325. https://doi.org/10.1016/S0013-7944(99)00076-4.

[15] Catel, E., Dahl, A., Lorentz, E., Besson, J. (2023). Coupling of a gradient-enhanced GTN model to the Beremin model for the simulation of ductile-to-brittle transition. In 15th International Conference on Fracture (ICF15), June 11-16 2023. Atlanta, GA USA.

[16] Iza-Mendian, A. & Gutierrez, I. (2013). Generalization of the existing relations between microstructure and yield stress from ferrite–pearlite to high strength steels. *Materials Science & Engineering A.* 561, 40-51. https://doi.org/10.1016/j.msea.2012.10.012.

[17] Pickering, F.B. (1978). *Physical Metallurgy and the Design of Steels.* London: Applied Science Publishers Ltd.

[18] Bruce, D., Paradise, P., Saxena, A., Temes, S., Clark, R., Noe, C., Benedict, M., Broderick, T. & Bhate, D. (2022). A critical assessment of the Archimedes density method for thin-wall specimens in laser powder bed fusion: Measurement capability, process sensitivity and property correlation. *Journal of Manufacturing Processes*. 79, 185-192. https://doi.org/10.1016/j.jmapro.2022.04.059.

[19] Hayu, R., Sutanto, H. & Ismail, Z. (2019). Accurate density measurement of stainless steel weights by hydrostatic

weighing system. *Measurement* 131, 120-124. https://doi.org/10.1016/j.measurement.2018.08.033.
[20] Park, J.J. (2018). Prediction of Void Closure in Metal Forming: One Cylindrical Through-hole. *ISIJ International*. 58(6), 1102-1107. http://dx.doi.org/10.2355/isijinternational.ISIJINT-2018-037.
[21] Chen, F., Zhao, X., Chen, H. & Ren J. (2020). Void closure behavior during plastic deformation using the representative volume element model. *Applied Physics A*. 126, 685, 1-13. https://doi.org/10.1007/s00339-020-03881-z.
[22] Zhang, M.X. & Kelly, P.M. (2009). The morphology and formation mechanism of pearlite in steels. *Materials Characterization.* 60(6), 545-554. https://doi.org/10.1016/j.matchar.2009.01.001.
[23] Verhoeven, J.D. & Gibson, E.D. (1998). The divorced eutectoid transformation in steel. *Metallurgical and Materials Transaction A*. 29(4), 1181- 1189. https://doi.org/10.1007/s11661-998-0245-4.
[24] Pandit, A.S. & Bhadeshia, H.K.D.H. (2012). Divorced pearlite in steels. *Proceedings of the Royal Society A: Mathematical, Physical and Engineering Sciences.* 468(2145), 2767-2778. DOI: 10.1098/rspa.2012.0115.
[25] Yasuda, T. & Nakada, N. (2021). Effect of carbon concentration in austenite on cementite morphology in pearlite. *ISIJ International.* 61(1), 372-379. https://doi.org/10.2355/isijinternational.ISIJINT-2020-325.
[26] Andrews, K.W. (1965). Empirical formulae for the calculation of some transformation temperatures. *Journal of the Iron and Steel Institute*. 203, 721-727.
[27] Kim, H., Inoue, J., Okada, M. & Nagata, K. (2017). Prediction of Ac_3 and martensite start temperatures by a data-driven model selection approach. *ISIJ International*. 57(12), 2229-2236. https://doi.org/10.2355/isijinternational.ISIJINT-2017-212.
[28] Wei, S. & Lu, S. (2012). Effects of multiple normalizing processes on the microstructure and mechanical properties of low carbon steel weld metal with and without Nb. *Materials and Design*. 35, 43-54. https://doi.org/10.1016/j.matdes.2011.09.065.
[29] Senk, D., Engl, B., Siemon, O. & Stebner, G. (1999). Investigation of solidification and microsegregation of near-net-shape cast carbon steel. *Steel Research*. 70(8-9), 368-372. https://doi.org/10.1002/srin.199905655.
[30] Ueshima, Y., Mizoguchi, S., Matsumiya, T. & Kajioka, H. (1986). Analysis of Solute Distribution in Dendrites of Carbon Steel with δ / γ Transformation during Solidification. *Metallurgical Transactions B.* 17, 845-859. https://doi.org/10.1007/BF02657148.
[31] Garbarz, B. & Pickering, F.B. (1988). Effect of pearlite morphology on impact toughness of eutectoid steel containing vanadium. *Materials Science and Technology*. 4 (4), 328-334. https://doi.org/10.1179/mst.1988.4.4.328.
[32] Naylor, J.P. (1979). The influence of the lath morphology on the yield stress and transition temperature of martensitic – bainitic steels. *Metallurgical Transaction*. 10A, 861-873. https://doi.org/10.1007/BF02658305.
[33] Uthaisangsuk, V., Prahl, U. & Bleck, W. (2011). Modelling of damage and failure in multiphase high strength DP and TRIP steels. *Engineering Fracture Mechanics.* 78, 469-486. https://doi.org/10.1016/j.engfracmech.2010.08.017.
[34] Lin, M, Yu, H., Ding, Y., Olden, V., Alvaro, A., He, J. & Zhang Z. (2022). Simulation of ductile-to-brittle transition combining complete Gurson model and CZM with application to hydrogen embrittlement. *Engineering Fracture Mechanics.* 268, 108511 1-16. https://doi.org/10.1016/j.engfracmech.2022.108511.